Hindawi
Geofluids
Volume 2022, Article ID 6872983, 11 pages
https://doi.org/10.1155/2022/6872983

Research Article

Characterization and Modelling of Multiscale Natural Fractures in Shale Reservoirs: A Case Study from a Block in the Southern Sichuan Basin

Shaohua Gai,[1] **Ailin Jia**,[2] **Yunsheng Wei**,[2] **and Ruohan Liu**[2]

[1]*CNOOC Research Institute Ltd, Beijing 100028, China*
[2]*Research Institute of Petroleum Exploration and Development, CNPC, Beijing 100083, China*

Correspondence should be addressed to Ruohan Liu; lrhsuper@163.com

Received 8 March 2022; Accepted 17 August 2022; Published 7 October 2022

Academic Editor: Yuxiang Zhang

Natural fractures are vital to the efficiencies of drilling and completion operation. The purpose of this paper is to characterize and model multiscale natural fractures in shale reservoirs. Based on the seismic and log responses, as well as outcrop and core observations, we divide natural fractures into Macro, Meso, and Micro three scales. Macroscale fractures are the faults picked directly in seismic profiles. Also, Mesoscale fractures are the natural fracture corridors analyzed by ant tracking technique in 3D seismic data. Furthermore, Microscale fractures are the fractures observed in imaging logs and cores. The fracture intensity is obtained by the correlation between ant tracking attributes and fracture density in borehole. The fracture aperture, dip, and azimuth are three main parameters, which are recognized by the loggings and cores. Stochastic modelling is applied to factures. We find that faults identified by the ant tracking result are excellent in line with Macroscale faults interpreted directly from seismic data. In addition, Mesoscale fractures are indicated from the ant tracking result, which are in accord with breakpoint in the well and in keeping with tectonic history of the area. Such high consistency indicates the ant tracking result is reliable. Moreover, image logs and cores reveal that it mainly develops high angle natural fractures and the fracture aperture is about 1 mm. The fracture strike includes three sets (NNW-SSE, NE-SW, and NNE-SSW). The distribution of the natural fractures in discrete fracture network (DFN) system is distributed controlled by the ant tracking result. Comparing the histograms of DFN results and fracture characterized by seismic and logging responses, as well as outcrop and core observation, it suggests that the major part of the observed natural fractures is retained into our DFN model.

1. Introduction

The physical properties of shale reservoirs are extremely poor, and it is necessary to form a network fracture system through volume fracturing to achieve economic and effective development. Natural fractures are the basis for the formation of complex fracture networks [1–5]. Fracture characterization and modelling of shale reservoir is the key to the rational design of shale gas horizontal well drilling and completion [6–9] and accurate evaluation of reservoir productivity [10–14].

For the identification methods [15–18], and characterization [19–22] parameters of natural fractures, the predecessors have done sufficient research and discussion. Zhang et al. [23] gave an overview of shale fracture types, formation mechanism, identification methods, and fracture parameters. Characterization parameters include occurrence, length, spacing, etc. Identification methods include geological methods, logging methods, seismic methods, and tectonic stress modelling. Of course, large-scale fractures have a great impact on industrial drilling and fracturing, which is mainly identified by seismic data [24]. Research on faults identified by seismic data has a long history. Marfurt et al. [25] proposed a spatial or temporal sliding multitime window method to estimate the seismic dip and azimuth, which provided a more robust method basis for the identification of fault anomalies, and also provided better basic data for fracture description algorithms such as structural steering filtering and coherent amplitude gradient. Pedersen et al. [26], Randen et al. [27], Van et al. [28] and Sun et al.

[29] all proposed ant tracking algorithm, which calculates ant body on the basis of inclination, variance, and other attributes. This method is widely used in the world. With the further application of ant tracking technology in complex fracture identification and carbonate rock fracture research [30, 31], the poststack prediction technology of fractures has made great progress in making full use of ant tracking attributes. The research on fracture anisotropy predicted by multiattribute fusion and its impact on oilfield development has been deepened [32, 33], and the ant tracking technology of prestack seismic data has also been fully utilized [34]. Hale [35] proposed the maximum likelihood attribute in the study of fault extraction and fault distance estimation, which improved the fault identification effect on the basis of enhancing the effect of fault seismic imaging; Ma et al. [36] used the maximum likelihood attribute to identify the Ordovician strike-slip fault in the Rewapu block in the Halahatang area, and achieved good application results.

Based on the current methods for modelling natural fractures in shale reservoirs, the modelling ideas of general fractured reservoirs are basically used, which can be divided into two categories: equivalent medium fracture modelling methods and discrete fracture network (DFN) modelling methods. Equivalent medium fracture models use simplified fracture descriptions (such as isotropic and parallel tabular fractures) to replace the actual fracture geometry and seepage characteristics, including dual media models, equivalent permeability models, and pipeline network models. It is represented by the dual medium model [37]. Using equivalent media to model fractures in shale gas reservoirs, the model fractures are not treated separately, which is easy to achieve reservoir simulation, but it is difficult to accurately describe the actual flow characteristics, and it cannot solve the problem of the multiscale of data from different sources [38], resulting in the loss of true details of many cracks. The discrete fracture network model (DFN) is an improvement to the continuous dual medium model, and is a deterministic or stochastic modelling by inputting parameters such as fracture distribution characteristics and geometric dimensions. In this method, each fracture is represented by fracture slices with different shapes, sizes, orientations, and dips in three-dimensional space. Multiple fracture slices with consistent characteristics form a fracture group, and multiple fracture groups form a fracture system [39]. The discrete fracture network model is rooted in stochastic simulation, and each fracture is built following the following rules: the shape of the fracture patch is a convex polygon (rectangular, elliptical, or more complex); the size of the fracture patch conforms to a known distribution (such as a negative exponential distribution); the location of the fracture obeys the spatial distribution function; and the orientation of the fracture is obtained by extracting the uniform or Fisher distribution [40]. Essentially, this simulation method is a target-based simulation that iterates over and over to make the final fracture distribution conform to given statistical characteristics.

When establishing the reservoir DFN model, the natural fracture modelling idea of shale reservoirs is mainly based on seismic ant tracking attributes, imaging logging, outcrop, and core observations for multiscale fracture modelling [41–43]. The constraints in DFN modelling can be the fracture density explained by logging, or the fracture density volume data obtained from seismic attributes [44, 45]. Shen et al. [46] modeled two-scale fractures composed of diffuse fractures and discrete fracture networks (DFN), and applied two-step calibration using well test data and streamline simulation to calibrate fracture aperture and density parameters. In addition, Mohaghegh [47] inferred the presence and the extent of the NFN from well productivity and all the measured parameters that impact it in Utica shale using artificial intelligence (AI).

As for the shale reservoirs in the southern Sichuan Basin, Wang et al. [48] just briefly analyzed the deformation characteristics and the stress field controlling the deformation by studying the paleotectonic evolution and the current structural characteristics of the southern Sichuan area, and comprehensively study the characteristics of the fractures in the Silurian Longmaxi Formation in the area, and discuss the development laws of fractures. Nevertheless, fracture modelling and forecast is not implemented. Jun et al. [49] used the prestack AVO integrated with Ant Tracking technique to detect and characterize NFSs and as inputs into Discrete Fracture Network (DFN) modelling to form a3D NFSs model. Liang et al. [50] focuses on characterizing the medium-scale fracture system with Ant Tracking technique. However, They did not describe the fractures in detail, nor did they establish a set of recommended methods and procedures for fracture modelling.

In this paper, fractures are characterized based on the seismic and log responses, as well as outcrop and core observations. Then deterministic and stochastic modelling are used for Macroscale, Mesoscale, and Microscale fractures to a Discrete Fracture Network (DFN) system. An integrated methods and procedures for fracture modelling is established.

2. Geological Settings

The block is located to the south of the Sichuan Basin, China (Figure 1). There are only three vertical exploration wells No. 1, 3, and 9 in and around the block, and other horizontal wells are production wells. The target layer is Wufeng (WF)-Longmaxi (L) Formation shale, and the lower part of the formation is deep-water shelf facies deposition. The Longmaxi Formation is divided into two parts from bottom to top, namely, L1 and L2. The lower L1 formation contains two subsections, L11 and L12. L11 is divided into 4 layers (1, 2, 3, and 4 layers) from bottom to top. The formation is dominated by quartz, calcite, and clay, with a lesser amount of feldspar, dolomite, and pyrite. The target black shale is organic-rich, which reveals that the shale has a good gas potential. There are four dominant reservoir space types, including organic matter pores, interparticle pores, intraparticle pores, and fractures [51]. The fractures in the Longmaxi Formation in study area are mainly high-angle fractures. Three groups of fault systems are developed in the target layer of the study area, which mainly occurred in the Yanshan-Xishan period. In the late Yanshan period, the tectonic curtain formed a near-S-N direction squeezing and formed a near-E-W direction fault. In the early Himalayas, the NNE-SSW direction squeezed to form the NNW-SSE direction fault. The mid-Hishan tectonic

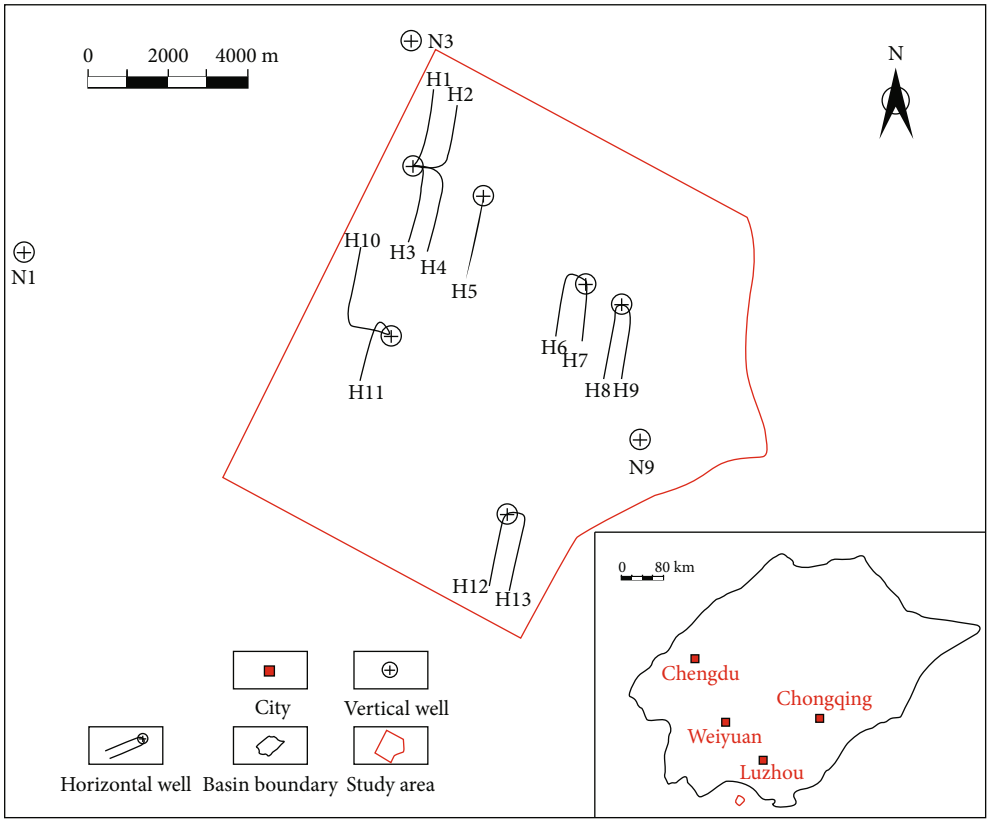

Figure 1: The study area and well sites.

curtain formed NWW-SEE direction compression and formed (N)NE ~ (S)SW direction faults [48].

3. Materials and Methods

3.1. Materials. The data includes conventional logging data and stratification data of all wells, cores of Well N1 and N3, and imaging logging data of Well N3. There is also the seismic data from the work area. Besides, there are outcrop observation data of predecessors [48].

3.2. Methods. Firstly, we divide natural fractures into Macro, Meso, and Micro three scales [52]. Macroscale fractures are the faults picked directly in seismic profiles. Also, Mesoscale fractures are the natural fracture corridors analyzed by ant tracking technique in 3D seismic data. Furthermore, Microscale fractures are the fractures observed in imaging logs and cores. Secondly, fractures are characterized on the seismic and log responses, as well as outcrop and core observations, including fracture intensity, length, aperture, dip, and azimuth. Thirdly, deterministic modelling is used for Macroscale fractures and Mesoscale fractures, and the correlation analysis between the fracture density obtained from the imaging log and the seismic ant tracking result is carried out to establish a unified fracture density. With this as a constraint, stochastic modelling is used for Microscale fractures to a Discrete Fracture Network (DFN) system.

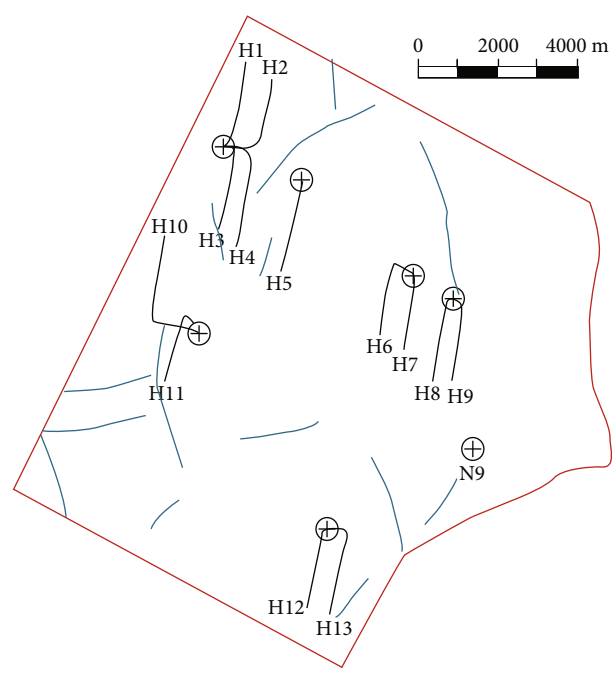

Figure 2: Faults system interpreted by seismic data in the study area.

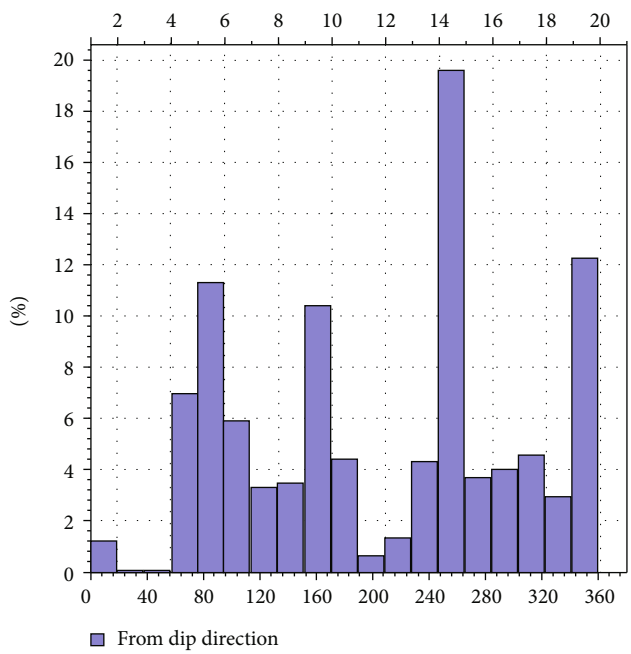

Figure 3: Histogram of fault azimuth distribution.

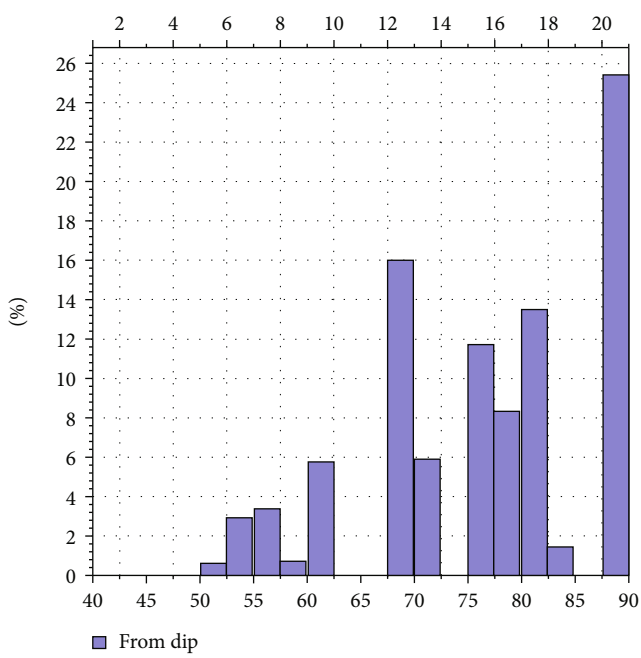

Figure 4: Histogram of fault dip distribution.

4. Results and Discussions

4.1. Characterization of Natural Fractures

4.1.1. Seismic Responses. The Macroscale faults interpreted directly from the seismic data in the study area can be roughly divided into three groups according to their strikes, namely, near E-W strike, (N)NE-(S)SW strike, and NNW-SSE strike (Figures 2 and 3). According to the seismic interpretation, the geometric occurrence of the fault is calculated, and Macroscale

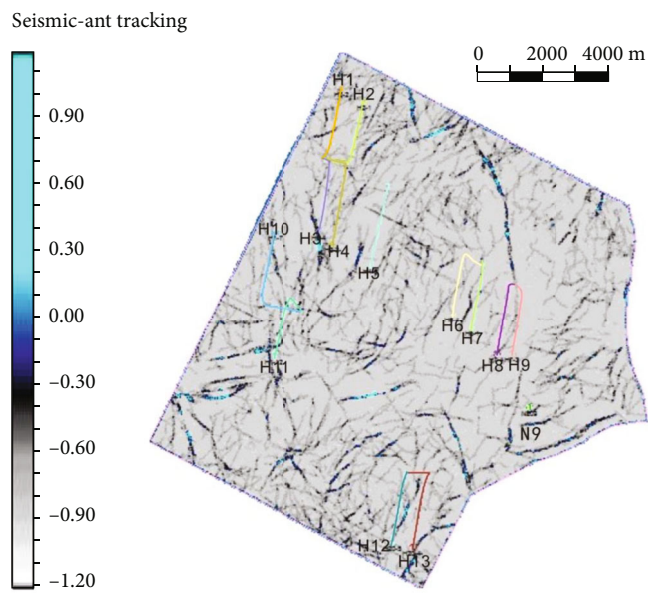

Figure 5: Ant tracking results.

fault is mainly high-angle (Figures 3 and 4). The results of seismic interpretation are consistent with the regional tectonic setting.

On the plane (Figure 5), we find that faults identified by the ant tracking result are excellent in line with Macroscale faults interpreted directly from seismic data above. In addition, Mesoscale fractures are indicated from the ant tracking result, which are in accord with breakpoint in Well H9. On the profile, H9 showed that the breakpoint at 4430 m corresponds well to Mesoscale fracture analyzed by the ant tracking (Figure 6). Such high consistency verifies the ant tracking result is reliable.

4.1.2. Outcrop Observation. The predecessors [48] observed the fractures of the Longmaxi Formation in the field outcrops around the study area. The fractures are described in detail, including the length, spacing, and occurrence.

(1) Fracture Length. The overall extension length of the fractures is approximately 3-10 meters, and the partial parallelism is good. Controlled by the thickness of the layer in shale, the length of the fractures is generally less than 2 m. Moreover, in the thicker ones, the fractures extending more than 6 m can be seen, and in the thick sandstone, there are also a few fractures with an extending length of more than 10 m (Figures 7(a) and 7(b)).

(2) Fracture Spacing. The outcrop in the field shows that there are mainly fractures which cut through the outcrop (Figures 7(c) and 7(d)). The fractures developed in the area have relatively small spacing, ranging from 0.1 to 0.5 m, which is mainly less than 0.4 m. In addition, the fracture length is 0.05-1.8 m, which is tightly closed, filled with calcite. The second is 0.4-1.2 m spacing, which tends to be south-east fractures, and the fractures in this direction cut each other into blocks.

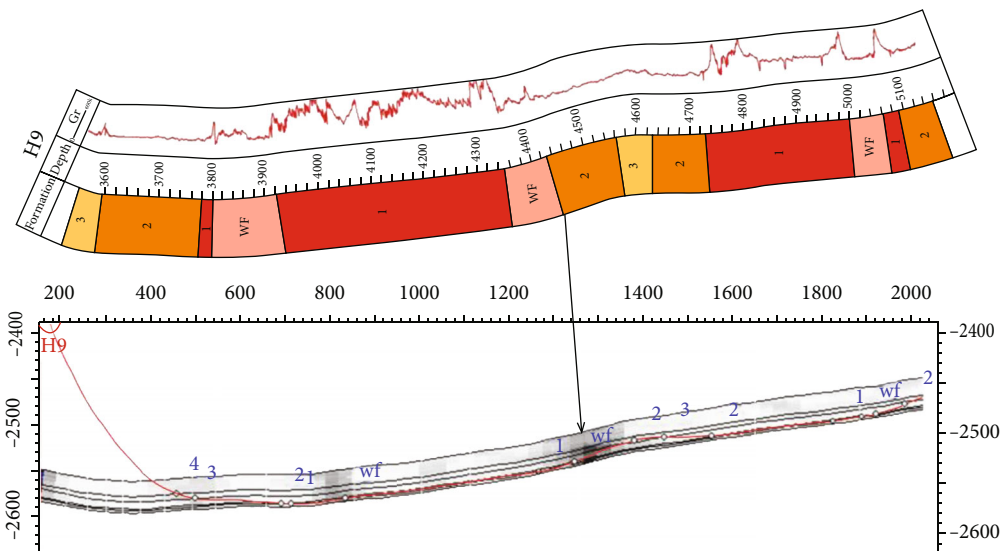

Figure 6: Profile of ant tracking in well H9.

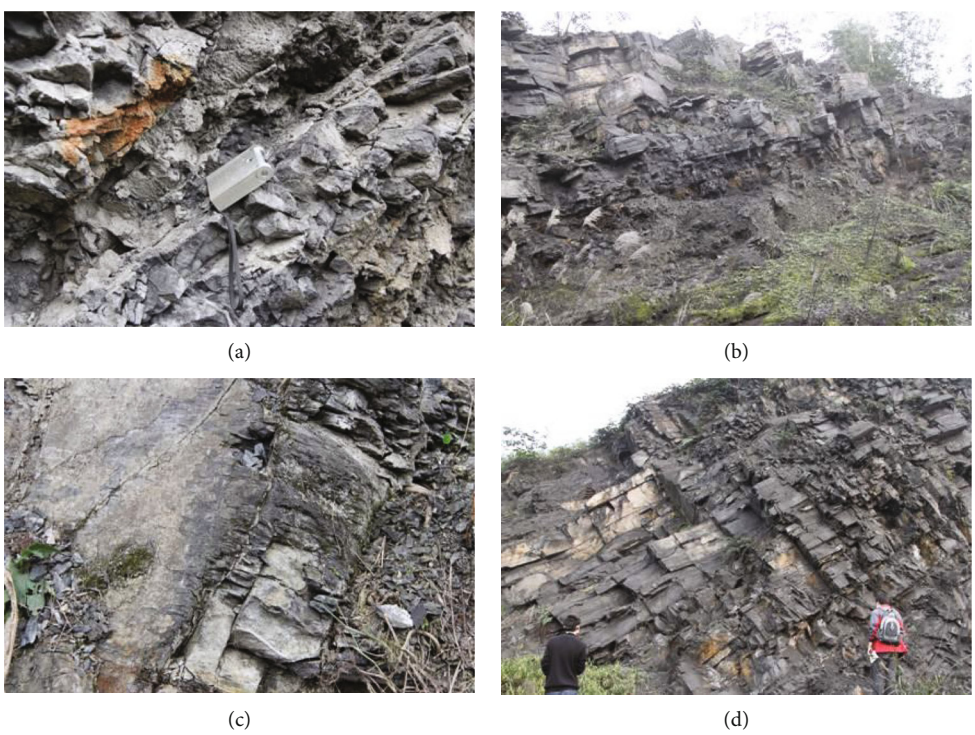

Figure 7: Fractures from the outcrop [48].

(3) Fracture Occurrence. Statistics of all the fractures in the Longmaxi Formation were used to make joint rose diagrams (Figure 8) and isodensity diagrams (Figure 9). The analysis of rose diagrams shows that the fracture (joint) dips (the green line) in the Longmaxi Formation mainly tend to be N2°-36°E, N51°-82°E, and E124°-274°W, followed by W346°-357°N. The joint dip angle (the blue line) of 30°-60° accounted for 52%, and the dip angle greater than 60° accounted for 48%. It can be seen that the dip angle of the joint in this area is dominated by the Medium-high angle. Meanwhile, the strikes (the red line) of the Longmaxi Formation fractures are developed at N30°-86°E, W273°-280 N°, and W315°-345°N. Besides, the joint isodensity map of Longmaxi Formation in this area shows that there are mainly three groups of dominant fracture (joint) groups developed in this area, namely 300°-355°∠45°-85°, 185°-210°∠5°-30°, 30°-90°∠30°-90°. In general, the Longmaxi Formation in study area has very well developed fractures, mostly with medium and high angle.

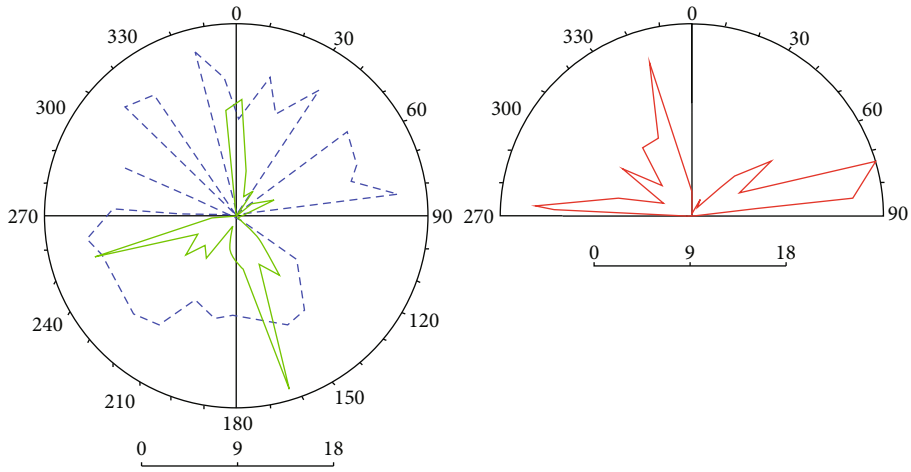

Figure 8: Longmaxi Formation's overall fracture (joint) dip rose diagram, and joint azimuth rose diagram [48].

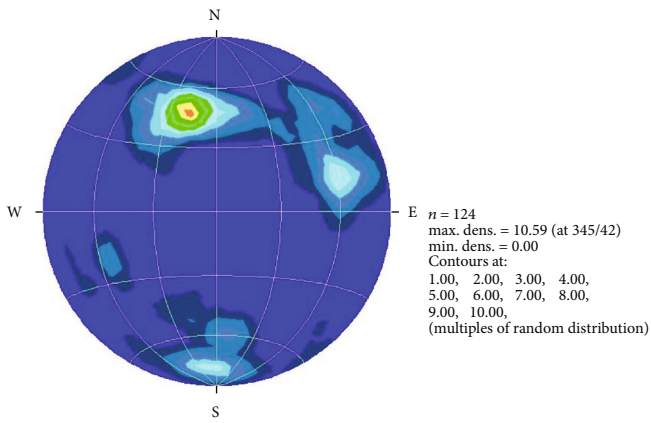

Figure 9: Fractures isodensity diagrams of Longmaxi Formation [48].

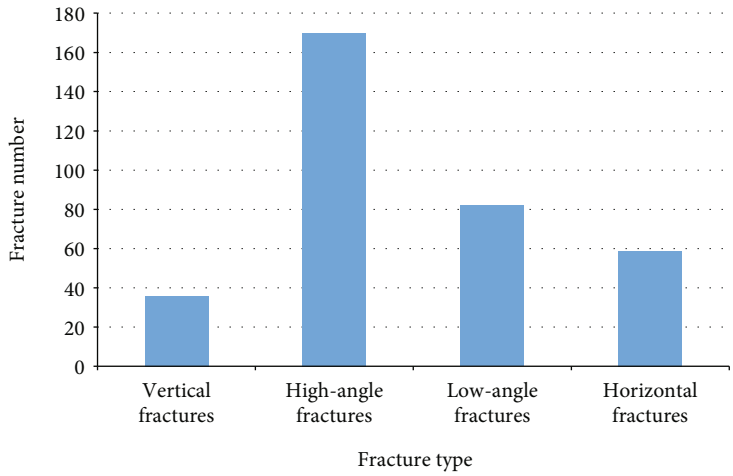

Figure 10: Type and number statistics of fractures [48].

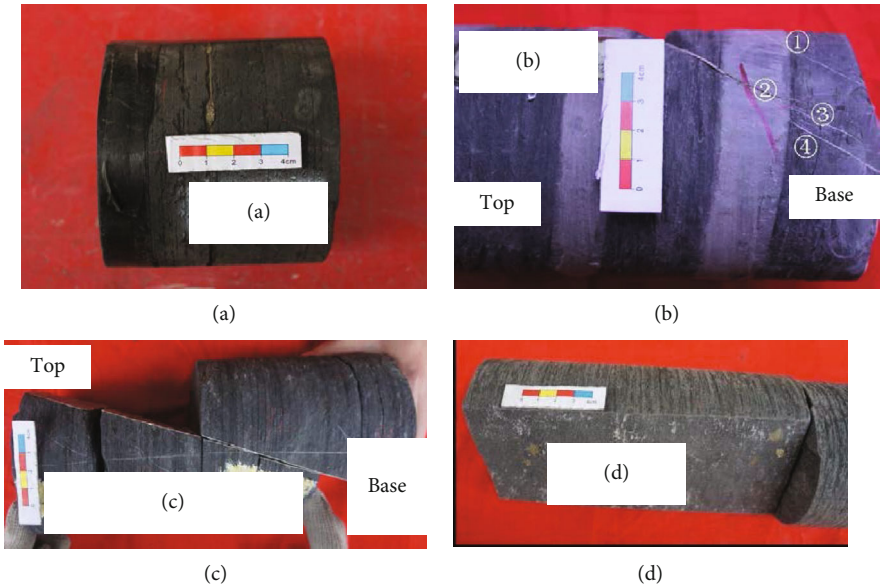

Figure 11: Fractures in the cores from Longmaxi Formation [48].

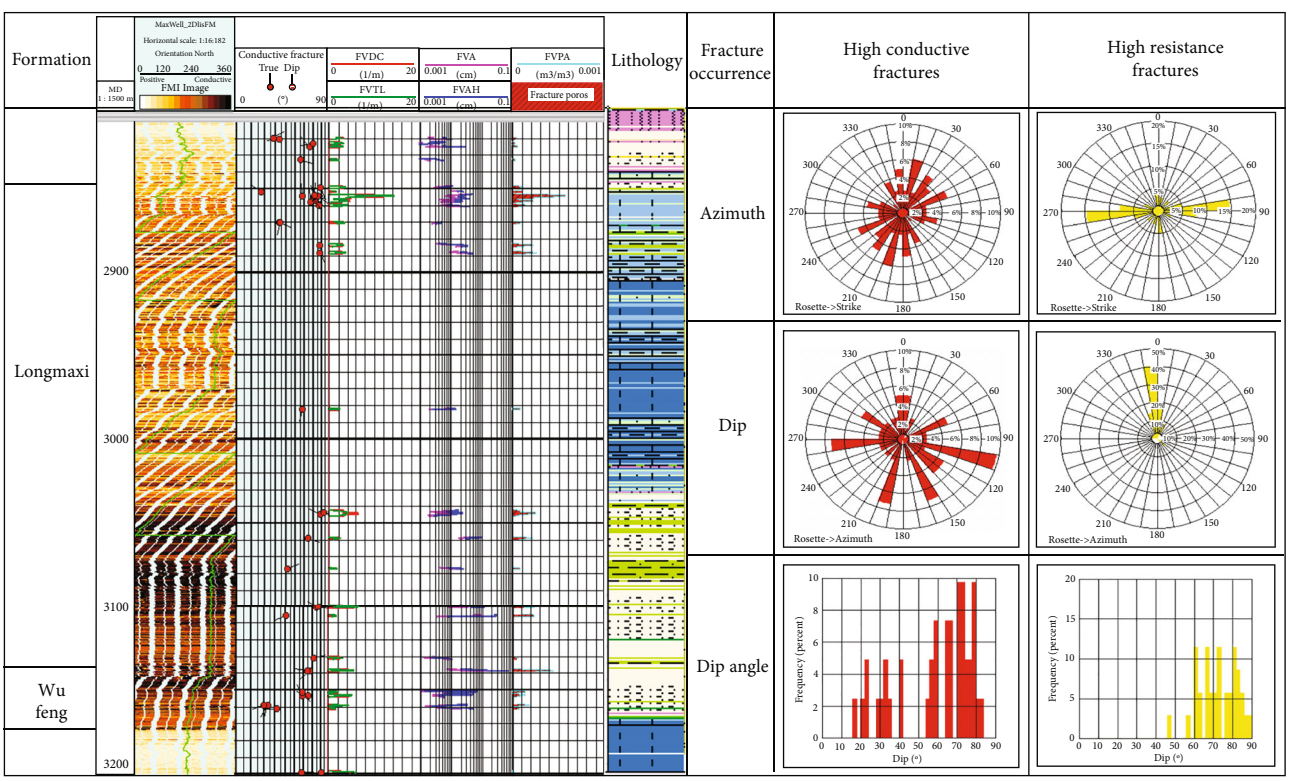

Figure 12: Fractures of Longmaxi Formation in FMI of Well N3.

4.1.3. Core Observation. The fractures in the Longmaxi Formation in study area are mainly high-angle fractures, accounting for 49% of all fractures. There are low-angle fractures, accounting for about 24%. Vertical and horizontal fractures are relatively less developed, accounting for 10% and 17%, respectively (Figure 10). The characteristics of fractures developed on the core of each well are as follows:

There are 7 horizontal fractures in the Longmaxi Formation of Well N1, with no vertical fractures, high-angle fractures, and low-angle fractures. In the core section of Well N1

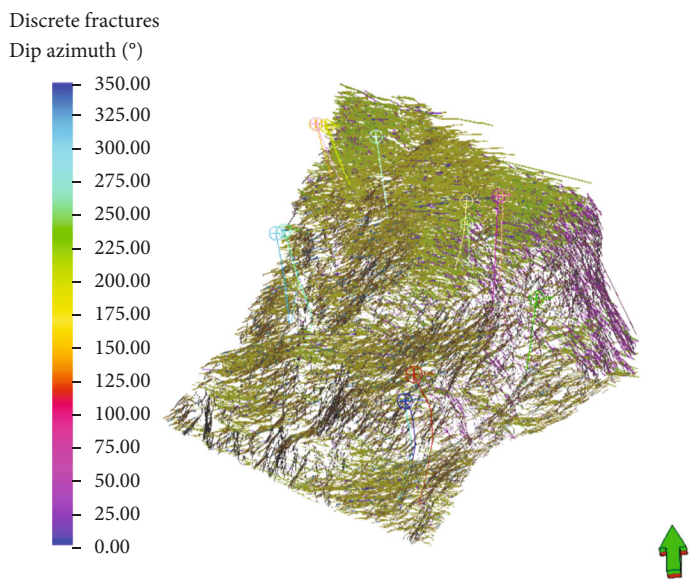

Figure 13: Discrete Fracture Network (DFN) constructed.

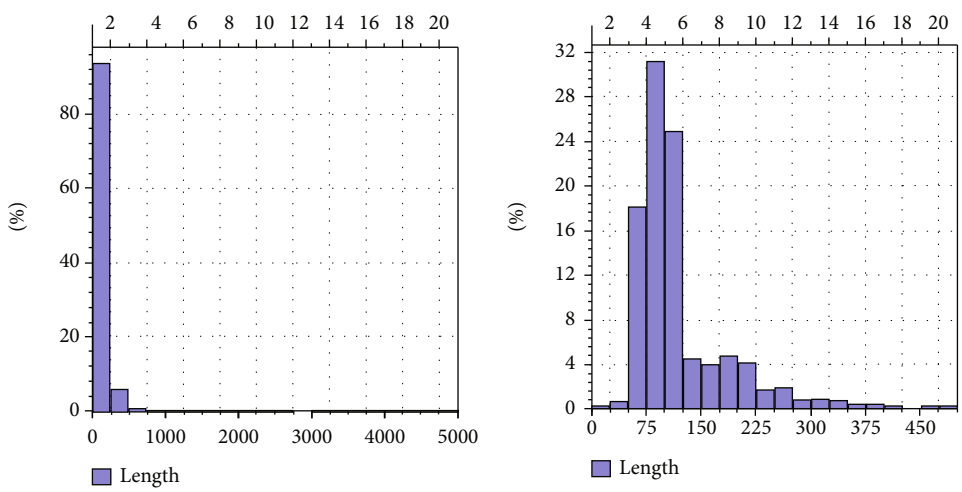

(a) Overall distribution of fracture length

(b) Concentrated distribution of fracture length

Figure 14: Histogram of fracture length distribution.

(2513.20~2513.30 m), it was found that there was a Longmaxi Formation seam at a distance of 1.6 m from the bottom, which was filled with pyrite (Figure 11(a)).

A group of 4 tightly closed fractures can be seen in the core section (2513.20~2513.30 m) of Well N3. The lengths of the 4 fractures are 4 cm, 8 cm, 4.5 cm, and 4.5 cm, respectively, and the dip angles are 75°, 70°, 67°, and 65°, respectively. The fracture width is about 1 mm. The fracture spacing is 1.7 cm, 0.4 cm, and 0.5 cm, respectively (Figure 11(b)).

There is a fracture in the core section (2228.28-2228.56 m) of Well N3, with a length of 28.1 cm and a dip angle of 75°, filled with calcite (Figure 11(c)). In the core section (2346.64-2349.31 m) of Well N3, there is a long-closed fracture with a length of 2.67 m, a vertical fracture with a dip angle of nearly 90° (Figure 11(d)).

4.1.4. Fullbore Formation MircroImager(FMI) Analysis. From Figure 12, FMI shows that fractures are relatively well developed in the Longmaxi Formation, and the fracture dip angles are middle-high, mostly concentrated at high angles. The strike can be roughly divided into three groups, namely, near E-W strike, (N)NE-(S)SW strike, and NNW-SSE strike, which are consistent with the strike trend of the Macroscale and Mesoscale fault in the study area.

4.2. Modelling of Natural Fractures. With the modelling method mentioned in section 3.2, natural fractures are modeled in the study area, and the distribution of fractures is shown in Figure 13.

Previous measurements of fracture lengths in multiple outcrop areas in other regions showed that most of the fracture

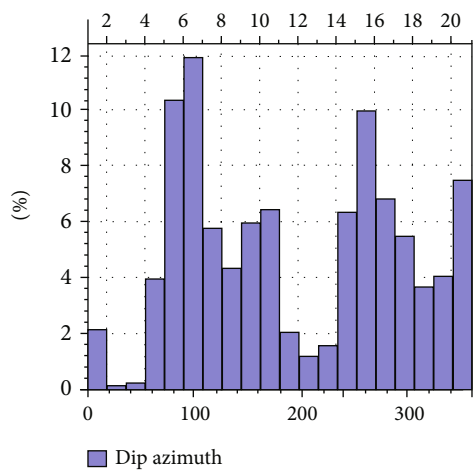

Figure 15: Histogram of fracture azimuth distribution.

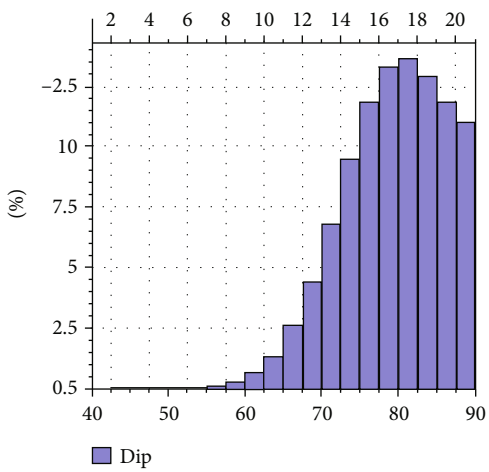

Figure 16: Histogram of fracture dip distribution.

lengths were less than 100 m. The length of natural fractures in the model is generally distributed below 5 km (Figure 14(a)), mainly concentrated below 150 m (Figure 14(b)).

The distribution of the fracture dip azimuth (Figure 15) is consistent with the Macroscale fracture shown in Figure 3. Simultaneously, the fracture dip angles are middle-high, mostly concentrated at high angles (Figure 16), which is the same as the previous dip angles described in Figure 4. The overall trend of the fracture dip azimuth and dip in the model is consistent with the previous geological understanding, which further verifies the correctness of the model.

5. Conclusions

(1) We divide natural fractures into Macro, Meso, and Micro three scales. Deterministic modelling is used for Macroscale fractures and Mesoscale fractures, and stochastic modelling is used for Microscale fractures to a Discrete Fracture Network (DFN) system

(2) Fractures are characterized on the seismic and log responses, as well as outcrop and core observations. The Macroscale and Mesoscale faults analyzed by the seismic data in the study area can be roughly divided into three groups according to their strikes, namely, near E-W strike, (N)NE-(S)SW strike, and NNW-SSE strike, with mainly high-angle dip. The log responses, outcrop, and core observations indicate that the fractures have relatively small spacing, mainly less than 0.4 m. The fracture width is about 1 mm

(3) Discrete Fracture Network (DFN) shows that the length of natural fractures in the model is generally distributed below 5 km, mainly concentrated below 150 m. Moreover, the fracture dip angles are middle-high, mostly concentrated at high angles. The overall trend of the fracture dip azimuth and dip in the model is consistent with the previous geological understanding, which further verifies the correctness of the model

Data Availability

All data, models, and code generated or used during the study appear in the article.

Conflicts of Interest

The authors declared no potential conflicts of interest with respect to the research, authorship, and publication of this article.

Acknowledgments

This study is funded financially with the Major National Science and Technology Projects (number-2017ZX05037-002; number-2016ZX05062002-003).

References

[1] X. Shang, S. Long, and T. Duan, "Current situation and development trend of fracture characterization and modelling techniques in shale gas reservoirs," *Natural Gas Geoscience*, vol. 32, no. 2, pp. 215–232, 2021.

[2] L. Zeng, W. Lyu, J. Li et al., "Natural fractures and their influence on shale gas enrichment in Sichuan Basin, China," *Journal of Natural Gas Science and Engineering*, vol. 30, pp. 1–9, 2016.

[3] T. Zhou, S. Zhang, Y. Feng, Y. Shuai, Y. Zou, and N. Li, "Experimental study of permeability characteristics for the cemented natural fractures of the shale gas formation," *Journal of Natural Gas Science and Engineering*, vol. 29, pp. 345–354, 2016.

[4] X. Xu, L. Zeng, H. Tian et al., "Controlling factors of lamellation fractures in marine shales: a case study of the Fuling area in eastern Sichuan Basin, China," *Journal of Petroleum Science and Engineering*, vol. 207, article 109091, 2021.

[5] A. Jia, Y. Wei, and Y. Jin, "Progress in key technologies for evaluating marine shale gas development in China," *Petroleum Exploration and Development*, vol. 43, no. 6, pp. 1035–1042, 2016.

[6] W. Qi, L. Xing, X. Chenggang, and L. Xun, "Geoscience-to-production integration ensures effective and efficient South

China marine shale gas development," *China Petroleum Exploration*, vol. 20, no. 4, p. 1, 2015.

[7] X. Jun, Z. Haomiao, S. Chaoyi, L. Qirong, F. Yu, and Y. Yang, "Practice of geology-engineering integration in Changning state shale gas demonstration area," *China Petroleum Exploration*, vol. 22, no. 1, 2017.

[8] W. Hu, "Geology-engineering integration-a necessary way to realize profitable exploration and development of complex reservoir," *China Petroleum Exploration*, vol. 22, no. 1, 2017.

[9] H. Tian, L. B. Zeng, X. Xu et al., "Characteristics of natural fractures in marine shale in Fuling area, Sichuan Basin, and their influence on shale gas," *Oil and Gas Geology*, vol. 41, no. 3, pp. 474–483, 2020.

[10] A. Jia, Y. Wei, C. Liu et al., "A dynamic prediction model of pressure-control production performance of shale gas fractured horizontal wells and its application," *Natural Gas Industry B*, vol. 7, no. 1, pp. 71–81, 2020.

[11] Y. Wei, Y. Qi, C. Jia, J. Yiqiu, and Y. He, "Production performance and development measures for typical platform horizontal wells in Weiyuan shale gas field, Sichuan Basin," *Natural Gas Industry*, vol. 39, no. 1, pp. 81–86, 2019.

[12] Y. Wei, J. Wang, Y. Qi, and Y. Jin, "Optimization of shale gas well pattern and spacing," *Natural Gas Industry*, vol. 38, no. 4, pp. 129–137, 2018.

[13] J. Wang, Y. Wei, and W. Luo, "A unified approach to optimize fracture design of a horizontal well intercepted by primary-and secondary-fracture networks," *SPE Journal*, vol. 24, no. 3, pp. 1270–1287, 2019.

[14] J. Wang, A. Jia, Y. Wei, W. Luo, and H. Yuan, "Semi-analytical simulation of transient flow behavior for complex fracture network with stress-sensitive conductivity," *Journal of Petroleum Science and Engineering*, vol. 171, pp. 1191–1210, 2018.

[15] S. Dong, L. Zeng, H. Cao, C. Xu, and S. Wang, "Principle and implementation of discrete fracture network modelling controlled by fracture density," *Geological Review*, vol. 64, no. 5, pp. 1302–1314, 2018.

[16] J. I. Ailin, "Research achievements on reservoir geological modelling of China in the past two decades," *Acta Petrolei Sinica*, vol. 32, no. 1, pp. 181–188, 2011.

[17] A. Jia, Z. Guo, J. Guo, and Y. Haijun, "Research achievements on reservoir geological modelling of China in the past three decades," *Acta Petrolei Sinica*, vol. 42, no. 11, p. 1506, 2011.

[18] L. Mu, G. Zhao, and Z. Tian, *Study on Reservoir Fracture Prediction*, Petroleum Industry Press, 2009.

[19] W. Ding, W. Zeng, R. Wang et al., "Method and application of tectonic stress field simulation and fracture distribution prediction in shale reservoir," *Earth Science Frontiers*, vol. 23, no. 2, p. 63, 2016.

[20] H. L. Kuo, "Geological analysis of ordovician fractured reservoirs in lunaan region of tarim basin," *Acta Petrolei Sinica*, 1995.

[21] W. Lyu, L. Zeng, Z. Liu, G. Liu, and K. Zu, "Fracture responses of conventional logs in tight-oil sandstones: a case study of the upper Triassic Yanchang formation in Southwest Ordos Basin, China," *China. AAPG Bulletin*, vol. 100, no. 9, pp. 1399–1417, 2016.

[22] W. P. Iverson, "Characterization of a naturally fractured chalk oil reservoir, silo, Wyoming," in *SEG Technical Program Expanded Abstracts 1990*, pp. 245–248, 1990.

[23] J. Zhang, S. Wang, X. Lu, and X. He, "Performance evaluation of oil displacing agents for primary-minor layers of the Daqing Oilfield," *Advances in Earth Science*, vol. 8, no. 1, pp. 79–86, 2011.

[24] Z. Ma, X. Yin, and Z. Zong, "Fracture parameters estimation from azimuthal seismic data in orthorhombic medium," *Journal of Natural Gas Science and Engineering*, vol. 100, article 104470, 2022.

[25] K. J. Marfurt, R. L. Kirlin, S. L. Farmer, and M. S. Bahorich, "3-D seismic attributes using a semblance-based coherency algorithm," *Geophysics*, vol. 63, no. 4, pp. 1150–1165, 1998.

[26] S. I. Pedersen, T. Randen, L. Sonneland, and O. Steen, "Automatic 3D fault interpretation by artificial ants," in *Conference Proceedings, 64th EAGE Conference & Exhibition*, Florence, Italy, 2002.

[27] T. Randen, E. Monsen, C. Signer et al., "Three-dimensional texture attributes for seismic data analysis," *Society of Exploration Geophysicists2000 SEG Annual Meeting*, pp. 668–671, Calgary, Alberta, 2000.

[28] P. P. Van Bemmel and R. E. F. Pepper, "Seismic signal processing method and apparatus for generating a cube of variance values," US Patent 6,151,555.2000-11-21.

[29] L. Sun, Z. Wang, and H. Li, "Application of fault tracking technology based on ant colony algorithm in wuxia area," *Fault-Block Oil & Gas Field*, vol. 21, no. 6, pp. 716–721, 2014.

[30] J. Wang, Y. Li, and L. Gan, "Fracture characterization based on azimuthal anisotropy of ant-tracking attribute volumes," *Oil Geophysical Prospecting*, vol. 48, no. 5, pp. 763–769, 2013.

[31] N. Li, L. Y. Wang, and S. B. Huang, "3D seismic fine structural interpretation in complex fault zones based on the high-definition ant-tracking attribute volume," *Oil Geophysical Prospecting*, vol. 54, no. 1, pp. 182–190, 2019.

[32] Q. Luo, J. Wang, and J. Luo, "Hypothesis outline of fracture-pore coupling enriching hydrocarbon on unconventional oil and gas," *Lithologic Reservoirs*, vol. 31, no. 4, pp. 1–12, 2019.

[33] L. Huo, J. Zhang, and L. Zheng, "Fault interpretation with multiple attributes in coalbed methane interpretation," *Oil Geophysical Prospecting*, vol. 49, no. S1, pp. 221–227, 2014.

[34] W. Bei, L. Xiangjun, S. Liqiang, X. Wei, L. Qian, and L. Han, "Multi-scale discrete fracture modelling technology for carbonate reservoir of Longwangmiao formation in Moxi area and its application," *Lithologic Reservoirs*, vol. 31, no. 2, pp. 124–133, 2019.

[35] D. Hale, "Fault surfaces and fault throws from 3D seismic images//SEG technical program expanded abstracts," *Society of Exploration Geophysicists*, vol. 2012, pp. 1–6, 2012.

[36] D. B. Ma, Y. M. Zhao, Y. T. Zhang, P. F. Yang, M. Yang, and L. Li, "Application of maximum likelihood attribute to fault identification: a case study of Rewapu block in Halahatang area, Tarim Basin, NW China," *Natural Gas Geoscience*, vol. 29, no. 6, pp. 817–825, 2018.

[37] J. E. Warren and P. J. Root, "The behavior of naturally fractured reservoirs," *Society of Petroleum Engineers Journal*, vol. 3, no. 3, pp. 245–255, 1963.

[38] X. L. Deng, J. H. Li, L. Liu, and K. X. Ren, "Advances in the study of fractured reservoir characterization and modelling," *Geological Journal of China Universities*, vol. 21, no. 2, p. 306, 2015.

[39] B. Wu, H. Tang, and T. Zhang, "An approach to discrete fracture network stochastic modelling-DFN model and DFM model," *Acta Geologica Sichuan*, vol. 30, no. 4, pp. 484–487, 2010.

[40] M. F. Benedetto, S. Berrone, S. Pieraccini, and S. Scialò, "The virtual element method for discrete fracture network simulations," *Computer Methods in Applied Mechanics and Engineering*, vol. 280, pp. 135–156, 2014.

[41] C. L. Cipolla, T. Fitzpatrick, M. J. Williams, and U. K. Ganguly, "Seismic-to-simulation for unconventional reservoir development," in *SPE Reservoir Characterisation and Simulation Conference and Exhibition*, Abu Dhabi, UAE, 2011.

[42] W. S. Bayer, M. Wunderle, E. Araujo et al., "Geological and geomechanical modelling of the Haynesville shale: a full loop for unconventional fractured reservoirs," in *Unconventional Resources Technology Conference, San Antonio, Texas, 1-3 August 2016. Society of Exploration Geophysicists, American Association of Petroleum Geologists, Society of Petroleum Engineers*, pp. 2112–2137, San Antonio, Texas, 2016.

[43] C. Du, X. Zhang, B. Melton et al., "A workflow for integrated Barnett shale gas reservoir modelling and simulation," in *Latin American and Caribbean Petroleum Engineering Conference*, Cartagena de Indias, Colombia, 2009.

[44] S. M. Peng, C. H. Suo, X. J. Wang, and X. L. Lang, "A modelling method for fractured reservoirs using multi-scale information," *Journal of Xi'an Shiyou University (Natural Science Edition)*, vol. 26, no. 4, pp. 1–6, 2011.

[45] X. Lang and S. J. Guo, "Fractured reservoir modelling method based on discrete fracture network model," *Acta Scientiarum Naturalium Universitatis Pekinensis*, vol. 49, no. 6, pp. 964–972, 2013.

[46] F. Shen, K. Zhao, Y. Zhang, Y. Yu, and J. Li, "Hierarchical approach to modelling karst and fractures in carbonate karst reservoirs in the Tarim Basin," in *Abu Dhabi International Petroleum Exhibition & Conference*, Abu Dhabi, UAE, 2019.

[47] S. D. Mohaghegh, "Mapping the natural fracture network in Utica shale using artificial intelligence (AI)," in *SPE/AAPG/SEG Unconventional Resources Technology Conference*, Austin, Texas, USA, 2017.

[48] S. Z. Wang, Z. Q. Li, M. Guo, and H. K. Li, "Developmental characteristics of Longmaxi formation shaly fissure in Changning of south of Sichuan area," *Science Technology and Engineering*, vol. 36, no. 13, pp. 10887–10892, 2013.

[49] Q. Jun, C. Xian, X. Liang, C. Zhao, G. Wang, and L. Wang, "Characterizing and modelling multi-scale natural fractures in the Silurian Longmaxi shale formation in South Sichuan Basin," in *Unconventional Resources Technology Conference*, pp. 2626–2637, Austin, Texas, 2017.

[50] X. Liang, X. Liu, H. Shu et al., "Characterization of complex multiscale natural fracture systems of the Silurian LongMaXi gas shale in the Sichuan Basin, China," in *SPE Asia Pacific Unconventional Resources Conference and Exhibition*, Brisbane, Australia, 2015.

[51] S. Gai, H. Liu, S. He et al., "Shale reservoir characteristics and exploration potential in the target: a case study in the Longmaxi formation from the southern Sichuan Basin of China," *Journal of Natural Gas Science and Engineering*, vol. 31, pp. 86–97, 2016.

[52] M. I. Al-Marzouqi, S. Budebes, E. Sultan, and I. Bush, "Resolving carbonate complexity," *Oilfield Review*, vol. 22, no. 2, pp. 40–55, 2010.